Synergies between Gaia, LSST and LISA

Isabella Danaliv

Lund Observatory
Lund University

2020-EXA170

Degree project of 15 higher education credits
June 2020

Supervisor: David Hobbs

Lund Observatory
Box 43
SE-221 00 Lund
Sweden

ASTK02

Synergies between Gaia, LSST and LISA
Astronomy, Bachelor's Degree Project

Author:
Isabella Danaliv
Supervisor:
David Hobbs

LUND
UNIVERSITY

June, 2020

Abstract

The scientific development of astronomy today mainly comes from the information that can be obtained via electromagnetic radiation. Today, the Gaia optical telescope is one of the most ambitious space projects man has ever completed. Another optical telescope LSST is designed to complement Gaia. In about 15 years it will also be possible to measure gravitational waves with the telescope LISA, which will detect binary stars, especially white dwarfs. Using gravitational waves will give completely different types of measurements.

It has also been found that a combination of the data from the two methods will give the possibility of a synergy effect, which means that it provides more information about the Universe than the sum of the information from each telescope. This is called multi-messenger astronomy, which in many areas has resulted in a remarkable development of opportunities in recent years (Egberts (2020)).

Synergy effects will make it easier to identify objects and reduce uncertainty in distance. It gives the possibility to calculate extra values such as the mass of the respective stars in binaries. Multi-messenger astronomy will also help understand the historical evolution of stars, galaxies and dark matter.

Different reviews are presented on the possibility of performing multi-messenger detection by Gaia, LSST and LISA. They have been discussed in many different papers. The purpose of this thesis is to review these observations and find out what their synergies together give which could not be achieved alone.

Populärvetenskaplig beskrivning

Astronomins vetenskapliga utveckling kommer idag främst från den information som kan erhållas via ljusstrålning från teleskop. Det viktigaste är teleskopet Gaia, som är ett av de mest ambitiösa rymdprojekt som människan någonsin har genomfört. Det kartlägger över en miljard stjärnor med position, avstånd och rörelse. Genom Gaias observationer skapas den första realistiska bilden av hur vår galax, Vintergatan, ser ut. Gaia sköts upp av Europeiska rymdorganisationen och började genomlysningen av himlen 2014. Ett annat optiskt teleskop LSST, Large Synoptic Survey Telescope, är utformat för att komplettera Gaia genom att detektera ännu svagare objekt längre bort. Det är ett markbaserat teleskop som för närvarande byggs i Chile i ett samarbete mellan offentliga och privata organisationer.

Ett än mer avancerat projekt, som förväntas vara klart år 2034, ska ge möjlighet att mäta gravitationsvågor med teleskopet LISA, LaserInterferometer Space Antenna. Det kommer att upptäcka dubbelstjärnor, som kretsar runt samma tyngdpunkt och kommer mestadels att vara vita dvärgar. Även neutronstjärnor och svarta hål kommer att detekteras då de också är små och kan rotera snabbt. Att använda gravitationsvågor ger helt olika typer av mätningar. LISA kommer att kunna kartlägga och studera utvecklingen av dubbelstjärnor i Vintergatan, som utgör hälften av alla stjärnor från det vi vet hittills. Projekteringen leds av Europeiska rymdorganisationen med stöd från NASA.

Gaia, LSST och LISA mäter delvis samma föremål. För dessa kan en kombination av informationen från olika teleskop möjliggöra en synergieffekt. Det innebär att det ger mer information än summan av informationen från respektive teleskop. Detta kallas multi-budbärar-astronomi, som i många sammanhang har haft en enastående utveckling under de senaste åren.

Olika undersökningar har utförts om möjligheten att uppnå synergieffekter av dessa tre teleskop. De har diskuterats i många olika artiklar. I detta arbetet, har jag granskat dessa observationer för att sammanställa gemensamma resultat. Här visas metoder för att identifiera dubbelstjärnor, som har detekterats via Gaia och som kan förväntas detekteras även av LSST och LISA, för att kunna användas för multi-budbärar-astronomi. Likaså visas utförande av olika tester där teleskopens resultat jämförs samt beräkningar och förslag på synergieffekter. Det presenteras även hur Gaia och LSST kompletterar varandra.

Synergieffekter har visat sig att göra det lättare att identifiera objekt och minska felmarginaler angående avstånd. Det ger även möjlighet att beräkna extra värden, exempelvis dubbelstjärnors respektive massor. Multi-budbärar-astronomi kommer också att bidra till att förstå den historiska utvecklingen av stjärnor, galaxer och mörk materia.

Contents

1 The tree telescopes Gaia, LSST and LISA

Initially, the three telescopes Gaia, LSST and LISA are presented, showing how they work and what they can detect separately. The purpose is to provide background information for later discussion.

1.1 About Gaia

1.1.1 Introduction

Gaia (Fig. 1) is a space telescope that allows for a compilation of a Milky Way catalog of the stars, providing a 3D mapping of the position, distance, and motion of stars, exoplanets, comets and asteroids (Gaia Helpdesk (2020)). It measures everything from the position of small bodies in our solar system to the activity of distant quasars beyond the Milky Way (ESA 2020, Gaia fact sheet). In total, it has observed around 1.7 billion stars in the second data release (YouTube, Gaia astronomical revolution). Measuring fairly bright objects, Gaia is especially good at observing our Galaxy.

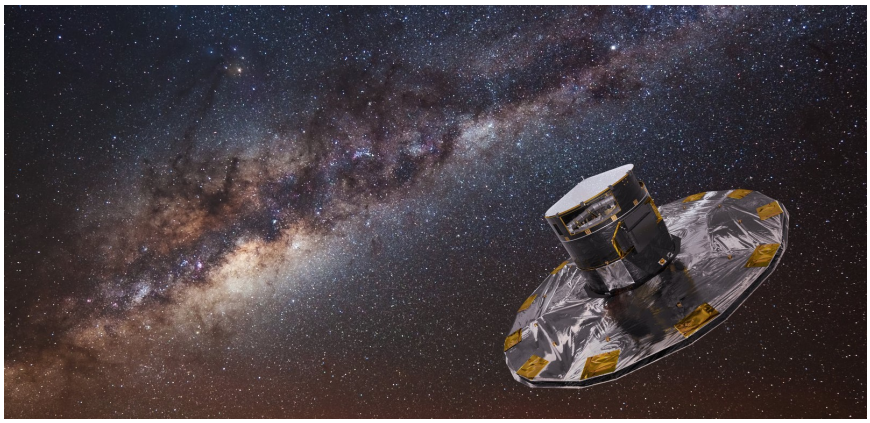

Figure 1: An artistic visualization of the space telescope Gaia where it scans the Milky Way (ESA 2020, Gaia news).

Gaia was launched by The European Space Agency, ESA, on December 19, 2013, beginning the scanning of the sky on July 25, 2014 (ESA 2020, Gaia DR2 primer). It is positioned in a orbit around the Sun-Earth L2 Lagrange point to maintain thermal stability (ESA 2020, Gaia fact sheet). With knowledge of the motion of the stars, we can simulate the Galaxy in unprecedented detail to study its overall dynamics and learn about its formation and evolution. Calculations using the data also indicates that some stars were born in another galaxy that has merged with a young Milky Way (YouTube, Gaia astronomical revolution). The measured values are fundamental to the research in astronomy, cosmology, relativity, dark matter and dark energy. Gaia is controlled by the European Space Operation Center (ESOC) in Germany and the European Space Agency (ESA) (ESA 2020, Gaia fact sheet).

Gaia is a sequel to the Hipparcos telescope, launched by ESA in 1989. It was the first space telescope with the mission to map the position and motions of stars. Gaia though has more advanced technology and 200 times more accurate measurement values (ESA 2020, Gaia summary).

1.1.2 Function and results

The different parts of Gaia are a mechanical and electrical service module in addition to a payload module that contains the instruments. In the payload module there are two primary mirrors at the entrance to the optical system housed on a Silicon carbide torus (ESA 2020, Gaia fact sheet). The focal plane has 106 detectors that rotate with the spacecraft. The detectors are of different types (Fig. 2):

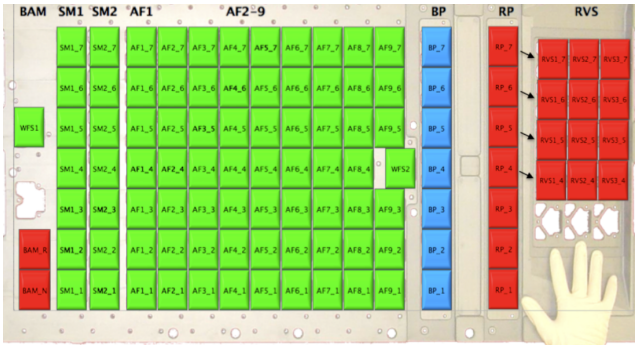

Figure 2: The focal plane contains the detectors Sky Mapper (SM), Astrometric field (AF), Blue Photometer (BP), Red Photometer (RP), and Radial Velocity Spectrometer (RVS) (van Leeuwen et al. (2017)), (Gaia Collaboration et al. (2016)).

- The detector "Sky Mapper" has one column of detectors for each field of view and measures the magnitude of the light and estimates how the light changes across the focal plane. The limit for how faint Gaia can detect is the magnitude 21. There is also a limit for bright stars, which is magnitude 3. Three other types of detectors described below use different methods to measure objects such as astrometry, photometry and spectrometry.

- The detector using astrometry is called "Astrometric Field" detector. Most of the detectors are of this kind and measure the wavelengths 330-1050 nm, which is a bandpass called the Gaia G band. They provide information on the flux of the stars, angular position and the proper motion of the stars. It also measures the parallax that is a useful method for distance in the Milky Way (described in chapter 5.1.3).

- The detectors using photometry are called "Blue and Red photometer" and measure the colour of the starlight in the two-colour bands. The blue photometer measures blue wavelengths 330-680 nm for objects having the magnitude called G_{BP}. The red photometer measures red wavelengths 630-1050 nm for objects having the magnitude called G_{RP}. This allows colour-magnitude diagrams to be made (described in chapter 4.2), from which you can measure temperature and extinction, which indicates the stage of development of stars. In addition, reddening can be measured, which indicates information about interstellar dust located in the line of sight between the star and Gaia.

- The detector using spectrometry is called "Radial Velocity Spectrometer" and measures low-resolution spectra. It is sensitive for the wavelengths 845–872 nm (ESA 2020, Gaia DR2 primer), which implies the 150 million brightest stars (ESA 2020, Gaia fact

sheet). It detects emission lines from both single and binary stars. Using the Doppler effect, the radial velocity can be calculated (ESA 2020, Gaia DR2 primer). The detailed information of the emission lines also describes the chemical composition and temperature of the star.

Each object has been observed on average 70 times by 2019. Gaia has continuously provided increasingly accurate average values with small error margins (ESA 2020, Gaia summary). The data is treated and released as a catalog in stages where the first is called Data Release 1 (Gaia DR1) for measurements taken between 25 July 2014 and 16 September 2015. Thereafter, the data was updated adding new measurements made up to 23 May 2016 and was released on 25 April, 2018, called Gaia DR2. It will later be followed by DR3 in the second part of 2021 and finally DR4. Gaia's fuel exceeds the need to complete the measurements that are planned for 2022 and can probably be extended to the end of 2024 (ESA 2020, Gaia DR2 primer).

1.2 About LSST

1.2.1 Introduction and results

The Large Synoptic Survey Telescope (LSST) (Fig. 3) has in January 2020 been renamed the Vera Rubin Telescope, after an astronomer who made discoveries about galaxy rotation rates and dark matter. It is a telescope that will scan space for about 10 years (LSST, About LSST) from its expected start in October 2022. The main difference from Gaia is that it specializes in measuring fainter light to detect what Gaia cannot detect, weaker than magnitude 20.7 which is mostly beyond the Milky Way. This implies that the focus is not just the Milky Way but also the understanding of the Universe as a whole. LSST can measure faint magnitudes to the limit of 27. The difference from other ground-based telescopes is that it is a wide-field (3 degree) survey telescope that automatically moves quickly and smoothly between the objects and repeatedly observes the same objects.

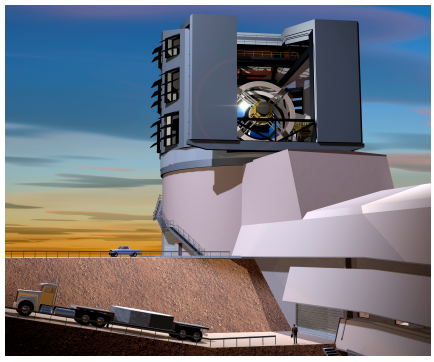

Figure 3: An artistic visualization of LSST, where the 8.4 m primary mirror is visible inside the protective housing (LSST, About LSST).

The result is essentially a film recording of the Universe. Billions of new objects will be discovered and monitored over time (LSST, General Public FAQs). It gives science an important tool to investigate high energy explosions, dark matter and dark energy. LSST will also detect dangerous asteroids and improve our understanding of the Milky Way structure.

An optical imaging telescope will provide a photographic image of the stars with tremendous detail (LSST, About LSST). LSST is synoptic, which means it sees all aspects of the objects as it observes everything with six different color filters with fast switches and it applies to a large volume of the Universe, which shows the Universe's time evolution since the distance to what we see in the Universe is related to time. With repeated photography, it also provides information about the change over ten years (LSST, General Public FAQs).

1.2.2 Technical structure

The telescope is ground-based and has three shaped mirrors that are 8.4, 5.0 and 3.4 m respectively (LSST, Mirror Design). The motion of the telescope is controlled by magnetic motors, which gives optimum mobility. The optics system makes it possible to continuously improve for optimal image quality (LSST, Telescope & Site).

The camera is a large-aperture, wide-field optical imager. It has 3 lenses, is 3 m in size and takes shots with 3200 megapixels of detail. It is the largest digital camera ever made. Light is seen from near ultraviolet to near infrared, which is particularly signified by distant objects with high redshift (LSST, Camera). Data management is an important part as it receives as much as 30 terabytes of data per night.

The light from the telescope's mirrors is corrected by lenses and then collected in the telescope's focal plane. Here are the detectors charge-coupled device (CCD) sensors, which work best in -100°C. The focal plane is behind the lenses in a vacuum container with electronics and thermal control (LSST, Focal Plane). Measuring the magnitude of light gives different ways to measure objects such as astrometry and photometry and spectrometry. Gaia can use all these methods as described but for LSST only 5 parameter astrometry and photometry will be available. Spectrometry, measuring Doppler, only works for very bright objects and that is not what LSST is aimed for.

Figure 4: LSST under construction in summer 2019 (LSST, Telescope & Site).

LSST is under construction (Fig. 4) in a collaboration between public and private organizations (LSST, Project Organization). It is built at a high geographical level to avoid clouds, at Cerro Pachon in north-central Chile, 100 km from civilization to avoid disturbances and light pollution (LSST, About LSST). A ground-based telescope limits us to seeing only half of the sky. However, since the Universe is assumed to be isotropic, it can be seen to represent the entire Universe. This type of telescope with such a large collection surface could not be made as a spacecraft. The data will be made available worldwide and benefit for a very broad research on the Universe. The expectations are high on everything we can learn from LSST (LSST, FAQs).

1.3 About LISA

1.3.1 Introduction

Laser Interferometer Space Antenna (LISA) is a space telescope, led by the European Space Agency with support from NASA (NASA, LISA). It is of a completely different nature than Gaia and LSST in that it does not measure light waves but instead gravitational waves according to Einstein's theory of gravity and spacetime. Gravitational waves are formed by the interaction of large masses that accelerate due to gravity. The waves move through spacetime at the speed of light (ESA 2018, Lisa Home).

Only since 1917 have we been able to detect this with ground built structures, such as LIGO and VIRGO. They detect distance differences, as a result of gravitational waves, created by the merging of two black holes or neutron stars (NASA, LISA). Gravitational waves permeate space but are weak, which is why they can best be detected in a completely still place, beyond the Earth's gravitational disturbances and noise (ESA, United space in Europe, LISA).

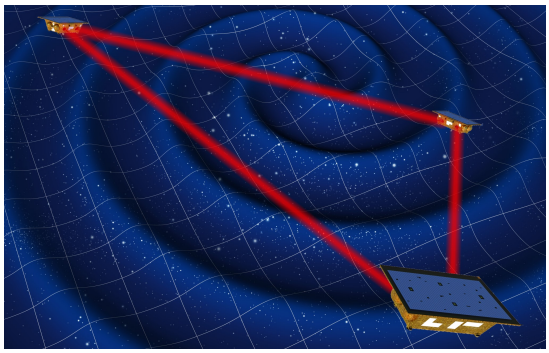

Figure 5: LISA consists of three spacecraft that measure gravitational waves, which create distortions in spacetime. They communicate with laser (ESA 2018, Lisa Home).

1.3.2 Function and results

LISA consists of three spacecraft that form an equilateral triangle, with respective distances 2.5 Gm, which is more than 6 times the distance to the moon. (ESA 2020, LISA). The distance between the spacecraft determines the detectable frequency range (ESA, United space in Europe, LISA). It is optimally adapted to be able to measure gravitational waves over a wide band of low frequencies from about 0.1 mHz to 0.1 Hz (ESA 2018, Lisa Home).

The three spacecraft have two telescopes each with associated optical systems and lasers. Two freely floating cubes of platinum and gold alloy in each spacecraft are like mirrors bouncing the lasers between the spacecrafts (Fig. 5). They have an interferometer in between them, where the waves are superimposed. The distance between all cubes is affected by gravitational waves and gives the measurement values of amplitude, direction and polarization. The polarization allows to determine the slope of the axis of the binary as the objects rotate (ESA, United space in Europe, LISA). Direction and distance can be measured, due to the relationship to the detectors' own rotation around the Sun. Then orbits, masses, quadrupole moments and redshifts can be calculated. With these data the evolution of binary stars in the Milky Way will be mapped and studied. Binaries make up half of all the

stars, though it is only those with short periods that can be detected by LISA, such as white dwarfs, neutron stars and black holes and combinations of them.

Another main goal is to know how and when supermassive black holes at the center of all large galaxies have been formed and grown and to reconstruct the Galaxy's development. It will be possible to study the formation of black holes and binary black holes as well as mergers (ESA 2018, Lisa Home). LISA will provide a developed understanding of tidal force and general relativity (ESA 2018, LISA Mission Description). It will detect massive black holes at high redshift z $\sim$ 12-20 that explains the Universe far away a very long time ago (Kupfer et al. (2018)). There are also hopes that it might be possible to detect the expansion of the Universe within the Big Bang (ESA 2018, LISA Mission Description). However, we do not fully know the limitations of LISA, but hope is high (ESA 2011, LISA FAQS).

LISA started as early as 1993 but since the gravitational wave observations 2017, it is more relevant and is under planning. By 2034, it is expected to be ready to be launched (ESA 2018, Lisa Home). The three parts will be in orbit around the Sun behind Earth, which implies a period of a year. They will have a so-called heliocentric path, which means that the triangular formation is maintained throughout this year's cycle (Fig. 6) (ESA, United space in Europe, LISA).

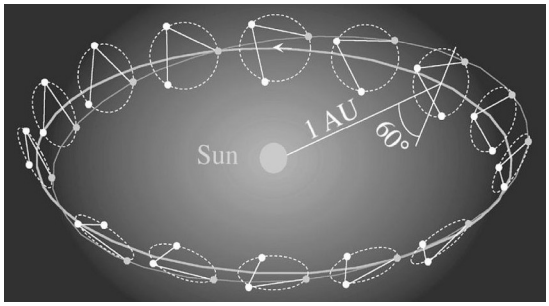

Figure 6: LISA's three parts in heliocentric orbit around the Sun, maintaining their triangular shape relative to each other (ESA, United space in Europe, LISA).

2 Gaia DR2 result with focus on binaries and white dwarfs

The purpose of this chapter is to provide background information on Gaia's measurement values and to provide increased understanding of how it can be applied to white dwarfs today.

2.1 Overview of Gaia DR2

At the beginning of the Gaia mission, there were various problems that caused interference, such as ice contamination from water trapped in the spacecraft before launch. The second Gaia data release, Gaia DR2 is thus significantly better than the first release, Gaia DR1. The uncertainties has diminished and it is fundamental to produce detailed studies. In addition to improved quality for Gaia DR2, the data is also taken over a longer period, with each object being observed at least five times. The content is more complete for making good calculations without using Gaia DR1 other than to make a comparison. The difference between

future data from Gaia DR3 and Gaia DR2 is not expected to be as large. Gaia DR2 is far from complete as it only contains 22 months of data. Measurements that are not good enough are neglected, for example, because they are too weak or are in bright crowded regions. The resulting values are divided into different sets, described below, mainly according to the previously presented measurement methods astrometry, photometry and spectrometry. Since LISA will only detect binaries, there are additional comments on these:

- Astrometric data set
  It contains measurement values for celestial position, parallax and proper motion. However, there is only the position for objects brighter than magnitude 21. In Gaia DR1, binaries were treated as if they were one object, so the proper motion, which was calculated from the center of the binary, then gave too low values for the individual stars. The proper motion and the parallax values are now better but can still be significantly wrong as binary motion is still not accounted for. In Gaia DR3, binaries will be treated as binaries and presented separately, giving much better results.

- Photometric data set
  Here are values for the apparent magnitude G and the effective color magnitude G_{BP} and G_{RP}. G-band fluxes are listed for all objects, while G_{BP} and G_{RP} exist only for 80% of objects and are the values used for colour-magnitude diagrams. This applies to stars that are not too faint, G < 21, and that are not in tight clusters.

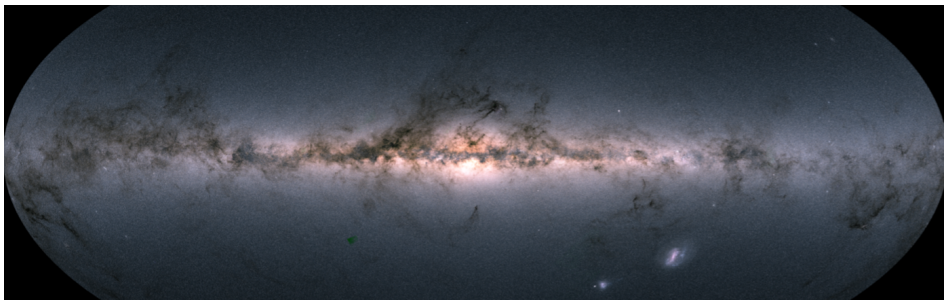

Figure 7: The total flux from photometric values for the G, G_{BP}, and G_{RP} bands provides a visual color image of the Milky Way. The uncertainty for the magnitude varies for different colors but has generally decreased in the Gaia DR2 (Gaia Collaboration et al. (2018b)).

- Radial velocity data set
  This information comes from spectrometry where the Doppler effect provides velocity and atmospheric information for the brightest stars. Binaries that have given double lines in spectroscopy have no value for radial velocity, but binaries that have one clear line and one weak are included, treated as single stars. In Gaia DR3, all types of binaries will be treated as binaries and get radial velocity values. The amount of measured values drops slowly between the magnitude 13-16.

- Astrophysical parameter data set
  Here are calculated values of the effective temperature T_{eff}, extinction A_G and reddening $E(G_{BP} - G_{RP})$, for stars brighter than magnitude 17. Extinction and reddening have very large uncertainty. Radius, and luminosity are also listed, calculated from T_{eff}.

- Variability data set
  It contains data on variable stars whose brightness changes, depending on whether the stars are intrinsic or extrinsic variables.

- Solar system data set
  It contains data that comes from all detected objects in our own solar system, which is over 14000 objects, mostly coming from the asteroid belt (Gaia Collaboration et al. (2018b)).

2.2 HR diagram

An important way of cataloging stars is using a Hertzsprung – Russell diagram (HR diagram) (Fig. 8). The vertical axis of the HR diagram is the absolute magnitude (M_G). It is defined in relation to the measured apparent magnitude (G) as

$$M_G = G - 5log_{10}(\frac{r}{10pc}), \tag{1}$$

where r is distance and p is the parallax, the measured angle difference in half of a year. The margin of error of parallax in Gaia DR2 is $4 \cdot 10^{-4}p$, which is less than 10 percent. The other axis of the diagram shows effective color, also called color index. It is defined as $G_{BP} - G_{RP}$ where BP represents a blue photometer and RP represents a red photometer (Lindegren & Hobbs (2018)).

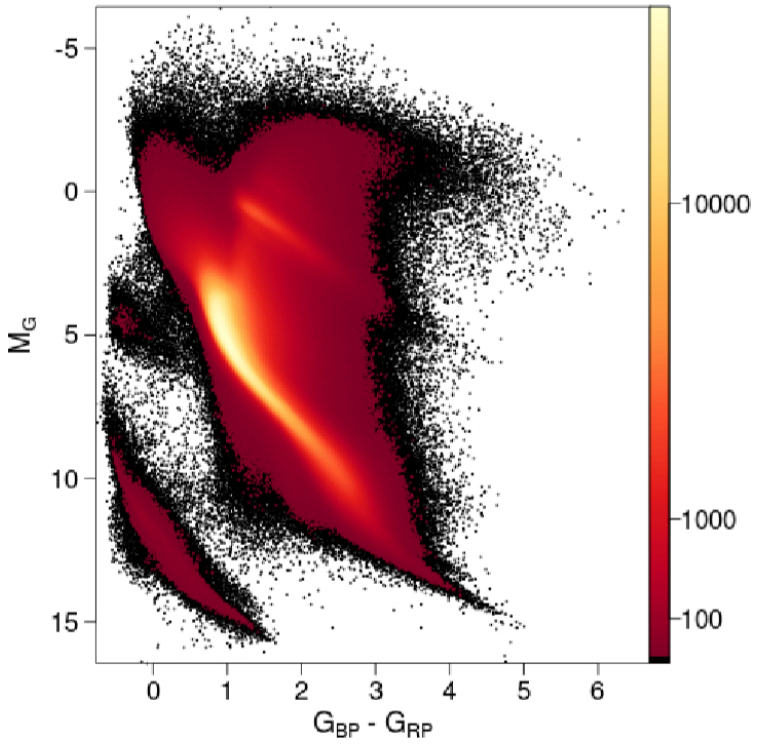

Figure 8: Total HR diagram from Gaia DR2 data. The axes' represent absolute magnitude (M_G) versus effective color $(G_{BP} - G_{RP})$. It tells the life stages of the stars of the Galaxy. The lighter part is the main sequence. The stars down to the bottom left are the white dwarfs (Gaia Collaboration et al. (2018a)).

The stars' respective positions in an HR diagram provide information about age, metallicity and kinematics and gives the classification and the evolutionary phase they are in (ESA 2020, The Gaia Hertzsprung-Russel Diagrams). The newborn stars are, among the red dwarfs, located at the bottom right. They are dark and reddish. The stars evolve along the HR diagram and eventually move to the red giant branch as they use up the hydrogen fuel. Most of the stars observed by Gaia DR2 are somewhere in this phase. It appears as a band from the bottom right of the chart to the upper left and is called the main sequence. Smaller stars have a long lifespan and stick to their lower part while massive stars quickly rise to the upper left of the chart. Thus, placement in the main sequence represents the respective ages of the stars. The lower ones can be older than 12 Gyr while the upper ones can be much younger than 1 Gyr.

The stars are in the main sequence for most of their existence while hydrogen is converted to helium in the center of the star. When the stars reach a certain age, depending on size and material composition, they leave the main sequence and move toward the top right of the chart to form red giants. The Sun is a good example of how a star is first located in the main sequence and then takes on different phases as other nuclear reactions take place (Fig. 9). Our sun will swell to a red giant star two times as it first uses up hydrogen fuel and later helium fuel. Then it will have a nebula phase, emitting glowing ionized gas before it is transformed into a white dwarf (Lindegren & Hobbs (2018)), (Schneider (2015)).

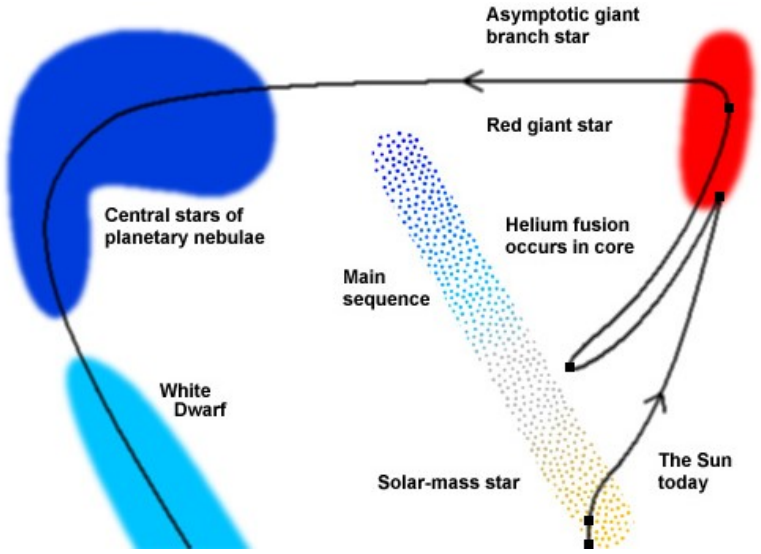

Figure 9: HR diagram, which illustrates the evolution of the Sun, from today being in the main sequence. Future development will turn it into a red giant and later a phase emitting gas before it turns into a white dwarf. All stars have a similar process (Centre for Mathematical Sciences, 5. Solar Evolution).

2.3 HR diagram for white dwarfs

Since LISA will detect white dwarfs, we will take a closer look at what HR diagrams tell about them. Values from Gaia DR2 show measurement values of parallax with an error margin of less than 5%, which gives very good values of the absolute magnitude. It provides an opportunity to study the HR diagram better than before. Fig. 10a shows a HR diagram

of the white dwarf cooling sequence. The orange line shows a significant concentration of stars of the size of 0.6 solar masses. Below this, one can distinguish a further concentration of the size of 0.8 solar masses, blue-marked. Yet another weaker concentration is the green dotted line.

To understand this separation, the stars can be studied in a color-color diagram, $G - G_{RP}$ versus $G_{BP} - G$, shown in Fig. 10b. Here the same separation occurs, which means that they have different atmospheric compositions. They are hydrogen, helium and carbon white dwarfs respectively. It has also been confirmed by comparison of another telescope, Sloan Digital Sky Survey (SDSS), which uses the spectroscopy method and is more sensitive to atmospheric compositions (Gaia Collaboration et al. (2018a)), (ESA 2020, The Gaia Hertzsprung-Russel Diagrams). In addition, above the orange line in the lower part of the HR diagram, it is possible to see another line. These are binary stars, which are slightly offset from the singular stars. Other stars between the white dwarf branches and the main sequence (Fig. 8) can also be binaries (YouTube, GaiaDR2 - A Guide for Scientists - DR2 Astrometry (part a)).

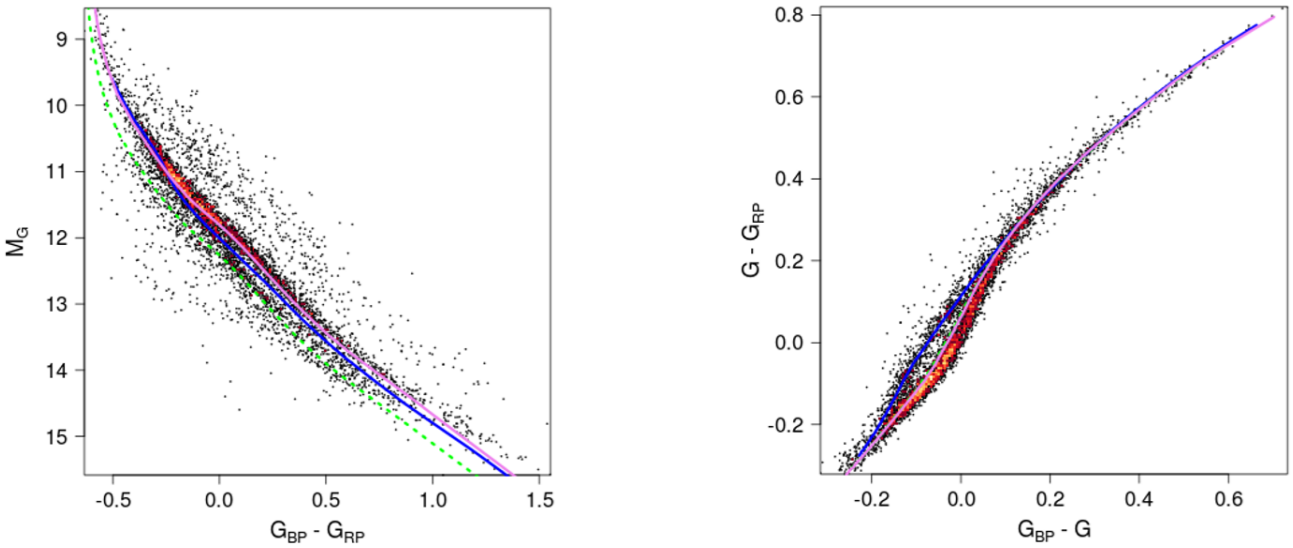

(a) **(b)**

Figure 10: (a) HR diagram from Gaia DR2 shows different concentrations of white dwarfs marked with different colors. (b) Color-color diagram show the same concentrations, which indicate that it is due to different atmospheric compositions, hydrogen (orange), helium (blue) and carbon (green) respectively for both figures (Gaia Collaboration et al. (2018a)), (ESA 2020, The Gaia Hertzsprung-Russel Diagrams).

3 Papers from V. Korol about Gaia, LSST and LISA

Gaia and LSST measure electromagnetic waves and LISA measures gravitational waves. Computer simulated studies have been conducted over the last few years on the multi-messenger effects of what the telescopes can contribute, how they complement each other and how their joint data can provide further information. Most papers on such projects that

are found in the international archive of scientific papers arxiv.org include the author Valeriya Korol. These are summarized below in chronological order to get an overview of the possibilities.

3.1 Encapsulation of the paper; LISA verification binaries with updated distances from Gaia Data Release 2

T. Kupfer, V. Korol, S. Shah, G. Nelemans, T. R. Marsh, G. Ramsay, P. J. Groot, D. T. H Steeghs, and E. M. Rossi, 2015 (Kupfer et al. (2018))

3.1.1 Introduction

Ultra-compact binary systems generate clear gravitational wave signals. They are two rotating astronomical objects with an orbital period of less than a few hours. It has previously been known that such binary systems, can be measured by LISA within the frequency bands LISA detects, 1 mHz - 1 Hz frequency bands. In 2018, Gaia DR2 was released containing information on position, parallax and motion for 1.3 billion objects with the focus on objects in the Milky Way. The paper presents a project to study these objects in more detail, to identify more binaries that LISA will be able to detect and to calculate expected results for the Milky Way. This project is made by the V. Karol team.

Binaries that can be detected both by optical telescopes and with LISA, called verification binaries, will give synergy possibilities. The resul predicted 16 verification binaries. 11 of them are AM Canum Venaticorum stars, AMCVn stars (Kupfer et al. (2018)), which are semidetached warm blue binary white dwarfs, where one of them accretes hydrogen-poor matter from the other (Onward to the edge, Binary Stars (Part I)) (described in Fig. 11). 4 of them are detached white dwarfs often called double white dwarfs, DWD (Korol & Rossi (2019)). Although detached binaries are the most common binaries, AMCVn binaries are more common as verification binaries since they are brighter. One hot subdwarf binaries have also turned out to be a verification binary. (Kupfer et al. (2018)), (Korol & Rossi (2019))

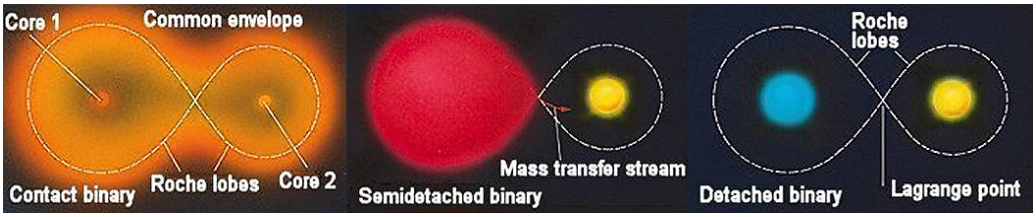

Figure 11: Detached binary means that the objects are separated with no mass transfer. Semidetached binary means that one of the objects has filled the Roche lobe transfer mass to the other due to the tidal effect. For contact binary, they have both filled their Roche lobe and transfer mass to each other (Onward to the edge, Binary Stars (Part I)).

3.1.2 Finding verification binaries and their parameters using Gaia DR2

In order to be able to predict gravitational waves of a binary system and calculate if it can be detected by LISA, their respective mass, orbital inclination, period and distance are needed.

The masses, radii and orbital inclination can be determined by spectroscopy and photometry using Gaia DR2. Though, the orbital inclination can only be poorly measured and only as edge-on and eclipsing binaries. For mass measurements in an AMCDn type binary, only advanced method for eclipsing binaries can be used because the accretion disc is visible in the spectrum and disturbs the observation of the two stars.

Assumptions for mass ratio and evolutionary stage are made, which reflects the uncertainty values. The masses of the 16 verification binaries and other properties are presented in a table, Fig. 12.

Source	l_{Gal} (deg)	b_{Gal} (deg)	Orbital period (sec)	m_1 ($M_\odot$)	m_2 ($M_\odot$)	ι (deg)
AM CVn type						
HM Cnc	206.9246	23.3952	321.529	0.55	0.27	≈38
V407 Vul	57.7281	6.4006	569.395	[0.8±0.1]	[0.177±0.071]	[60]
ES Cet	168.9684	–65.8632	620.21	[0.8±0.1]	[0.161±0.064]	[60]
SDSS J135154.46–064309.0	328.5021	53.1240	943.84	[0.8±0.1]	[0.100±0.040]	[60]
AM CVn	140.2343	78.9382	1028.73	0.68±0.06	0.125±0.012	43±2
SDSS J190817.07+394036.4	70.6664	13.9349	1085.7	[0.8±0.1]	[0.085±0.034]	10 - 20
HP Lib	352.0561	32.5467	1102.70	0.49-0.80	0.048-0.088	26-34
PTF1 J191905.19+481506.2	79.5945	15.5977	1347.35	[0.8±0.1]	[0.066±0.026]	[60]
CXOGBS J175107.6–294037	359.9849	–1.4108	1375.0	[0.8±0.1]	[0.064±0.026]	[60]
CR Boo	340.9671	66.4884	1471.3	0.67-1.10	0.044-0.088	30
V803 Cen	309.3671	20.7262	1596.4	0.78-1.17	0.059-0.109	12 - 15
Detached white dwarfs						
SDSS J065133.34+284423.4	186.9277	12.6886	765.5	0.247±0.015	0.49±0.02	$86.9^{+1.6}_{-1.0}$
SDSS J093506.92+441107.0	176.0796	47.3776	1188.0	0.312±0.019	0.75±0.24	[60]
SDSS J163030.58+423305.7	67.0760	43.3604	2389.8	0.298±0.019	0.76±0.24	[60]
SDSS J092345.59+302805.0	195.8199	44.7754	3883.7	0.275±0.015	0.76±0.23	[60]
Hot subdwarf binaries						
CD–30°11223	322.4875	28.9379	4231.8	0.54±0.02	0.79±0.01	82.9±0.4

Figure 12: The defined 16 verification binaries and their known physical properties, showing their location, orbital period, masses of the stars and inclination angle. The brackets show the data on mass and inclination angles that are based on assumptions. For references, see the report (Kupfer et al. (2018)).

3.1.3 Distance calculations using Gaia DR2

For most of the 16 binaries, the parallax (ϖ) is measured, which is used to calculate the distance (d) (Fig. 13 and 14). The same object is observed repeatedly during the year and the difference in position can be related to Gaia's movement around the Sun. The basic principle is simple geometry, but the calculations used are probability-based and more complex, since the distance depends on the uncertainty. Each measured value for parallax represents a probability distribution. A prior probability density, $P(d)$, contains an assumption of the distance distribution of the objects.

$$P(d) = \frac{d^2}{2L^3} exp(-d/L) \quad if \quad d > 0, \quad P(d) = 0 \quad otherwise. \tag{2}$$

$L > 0$ is a scale length constant. To determine posterior probability density, $P(d|\varpi, \sigma_\varpi)$, Bayes' theorem is used. It is a statistical theorem that describes the probability density of an event based on prior knowledge.

$$P(d|\varpi,\sigma_\varpi) = \frac{1}{Z}P(\varpi|d,\sigma_\varpi)P(d), \quad Z = \int_0^\infty P(\varpi|r,\sigma_\varpi)P(r)dr, \tag{3}$$

where Z is a normalization constant, σ_ϖ is an uncertainty of the measurement and $P(\varpi|d,\sigma_\varpi)$ is a likelihood function, which describes the probability of measuring parallax according to the parallax Gaussian

$$P(\varpi|d,\sigma_\varpi) = \frac{1}{\sqrt{2\pi}\sigma_\varpi} exp[-\frac{1}{2\sigma_\varpi^2}(\varpi - \frac{1}{d})^2]. \tag{4}$$

The prior probability density can be chosen so that the derivative of the posterior probability density is zero, to determine the mode of the posterior (Kupfer et al. (2018)). Then this equation can be solved and the distance can be calculated from the roots of the cubic equation (Bailer-Jones (2015)).

$$\frac{d^3}{L} - 2d^2 + \frac{\varpi d}{\sigma_\varpi^2} - \frac{1}{\sigma_\varpi^2} = 0. \tag{5}$$

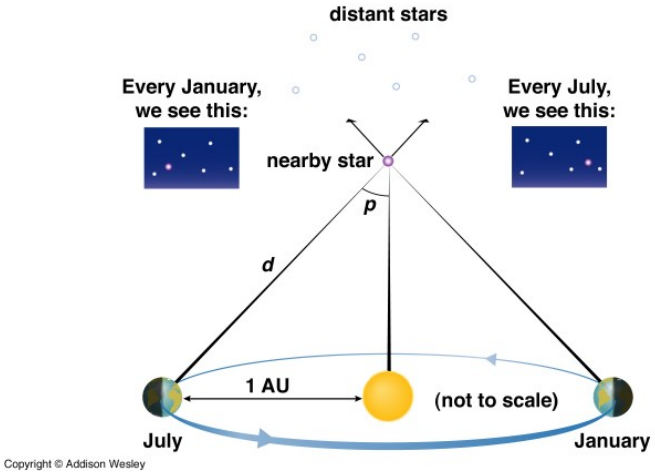

Figure 13: Parallax method for measuring distance. Since the Earth's orbital diameter is known the angle is measurable using the relation to the stars behind, the distance to the object can be calculated with simple geometry (Berkeley education, Lecture 13).

For the other binaries without parallax values the distance is estimated based on their flux, temperature and more, with a large margin of error. From Gaia, reliable distances are measured for the objects that are within a distance of a few hundred parsecs. The diameter of the Milky Way is approximately 30,000 parsecs which implies that the uncertainty becomes unreliable further away in the Galaxy.

3.1.4 Measured and derived parameters using Gaia DR2

LISA will detect gravitational waves with the amplitude (A) of the formula

$$A = \frac{2(GM_c)^{5/3}}{c^4 d}(\pi f)^{(2/3)}, \tag{6}$$

where f is the gravitational wave frequency and M_c is the chirp mass

$$M_c = (m_1 m_2)^{3/5}/(m_1 + m_2)^{1/5}, \tag{7}$$

a combination of masses from each star. The detected signal must be significantly clearer than the background noise. It is defined as the signal-to-noise ratio (SNR). By using the Gaia DR2 parallax, the project result gives a prediction of 52 verification binaries from the millions of binaries that LISA is expected to be able to detect. 11 of them are calculated to give SNR ≥ 20, 2 will give SNR ≥ 5 and 3 will give SNR ≈ 5. These 16 binaries are expected to be measured by LISA within a couple of months of searching and will be used to verify the performance of the instrument (Fig. 14). The values for SNR increase over time and are calculated from what LISA is expected to have detected within four years of measurements.

Source	f (mHz)	ϖ (mas)	σ_ϖ (mas)	d (pc)	σ_d (pc)	$\mathcal{A}$	SNR
AM CVn type systems							
HM Cnc	6.22	-	-	[5000]	-	6.4	211.1±3.18
V407 Vul	3.51	0.095	0.327	1786	667	11.0±5.9	169.7±2.17
ES Cet	3.22	0.596	0.108	1584	291	10.7±4.6	154.3±2.09
SDSS J135154.46–064309.0	2.12	0.596	0.313	1317	531	6.2±3.5	21.8±0.24
AM CVn	1.94	3.351	0.045	299	4	28.3±3.2	101.2±0.96
SDSS J190817.07+394036.4	1.84	0.954	0.046	1044	51	6.1±2.4	20.3±0.13
HP Lib	1.81	3.622	0.052	276	4	17.5±3.9	43.7±0.28
PTF1 J191905.19+481506.2	1.48	0.550	0.327	1338	555	3.2±1.8	4.0±0.02
CXOGBS J175107.6–294037	1.45	1.016	0.146	971	156	4.2±1.8	4.5±0.02
CR Boo	1.36	-	-	337^a	$^{+44\,a}_{-35}$	13.4±4.2	21.9±0.13
V803 Cen	1.25	-	-	347^a	$^{+32\,a}_{-27}$	16.0±5.4	26.2±0.17
detached white dwarfs							
SDSS J065133.34+284423.4	2.61	1.000	0.476	933	493	16.2±8.6	90.1±1.13
SDSS J093506.92+441107.0	1.68	-	-	645^b	41^b	29.9±7.7	44.9±0.31
SDSS J163030.58+423305.7	0.84	0.937	0.270	1019	357	11.5±4.9	4.6±0.03
SDSS J092345.59+302805.0	0.51	3.340	0.173	299	10	26.4±6.5	5.6±0.06
hot subdwarf binaries							
CD–30°11223	0.47	2.963	0.080	337	9	41.5±1.8	4.9±0.04

Figure 14: Result properties from the defined 16 verification binaries, showing parallax (ϖ) and calculated distance (d) with their uncertainty of measurement (σ). Also, their derived gravitational wave parameters are showed, such as frequency (f), the strongest expected gravitational wave amplitude (A), and signal-to-noise ratio (SNR) (Kupfer et al. (2018)).

The various parameters that LISA will provide are amplitude (A), frequency (f), polarization angle (ψ), orbital inclination (i), the sky location of elliptic latitude and longitude (θ, ϕ) and initial gravitational orbital wave phase (ϕ_0). The Fisher information matrix is used to calculate uncertainty for amplitude and inclination (Kupfer et al. (2018)). A Fisher information matrix describes the amount of information one input parameter carries about another output value (Mathematics Stack Exchange 2018, Mathematics, Fisher information matrix). Since distance is the parameter that causes the most uncertainty, it is only possible to make proper calculations for objects within a distance of a few hundred parsecs. A gravitational wave amplitude (A) with an error margin of 5 % - 10 % can be obtained for different types of objects. Other objects, which are further away, require more parameters to be able to predict amplitude (Kupfer et al. (2018)).

3.2 Encapsulation of the paper; Prospects for detection of detached double white dwarf binaries with Gaia, LSST and LISA

Valeriya Korol, Elena M. Rossi, Paul J. Groot, Gijs Nelemans, Silvia Toonen, and Anthony G.A. Brown, 2016 (Korol et al. (2017))

3.2.1 Introduction

The ultra-compact white dwarf binaries are very common in the Milky Way as predicted by numerical simulations. However, they are faint, which makes them difficult to detect. The first discovery was as late as 1988. With LISA they can provide research on white dwarfs, stars, and binaries and for providing a detailed 3D map of the Milky Way. This paper describes how to simulate the population of white dwarf binaries in the Milky Way and how to make estimates on which binaries will be detected by the telescopes. It is also made by the V. Korol team.

3.2.2 Simulation of population

The population of white dwarfs binaries was computer simulated including contact, semi-detached and detached binaries (described in Fig. 11). To achieve a credible result, reliable parameters for a predicted Galactic population were created, such as assuming a binary fraction of 50% and creating probable mass-ratio distribution, thermal eccentricity, orbital separation and inclination angle. For the simulation, two different scenarios for phases of mass transfer were used, which gave different results, offering a good test for binary evolution studies. In one scenario, the total conservation of the orbital energy is assumed. In the second scenario, an initial loss of energy in the form of mass and angular momentum is assumed. For the energy loss scenario, twice as many binaries were created as they were for the conserved energy scenario. The result also showed that for those who lost energy there was a wider range of mass ratio distribution with decreasing orbit. Those who instead conserved the energy had a mass ratio of about 0.5. A deeper description of the two models is given in the paper. The scenario used for the figures and diagrams below is with the loss of energy in the form of mass and angular momentum, since it is the most common situation. What was not simulated, that could give more trustworthy results, would be a model with a reliable balanced combination of both scenarios.

3.2.3 Binaries detected by Gaia and LSST

New discoveries expected by Gaia and LSST are primarily white dwarf binaries. Most white dwarfs in the Galaxy are too weak to be detected by Gaia. LSST is expected to be able to complement Gaia but only over half of the sky since the telescope is ground-based. Gaia and LSST cover about the same wavelengths. LSST will make measurements on each object much more frequently, once every 3 days, and is expected to observe each object 10^3 times in total. Gaia, which only observes each object once per 26 days, has only detected each object about 70 times in 2019, which was the expected total amount. However, Gaia's life span has been extended. More observations result in lower uncertainties.

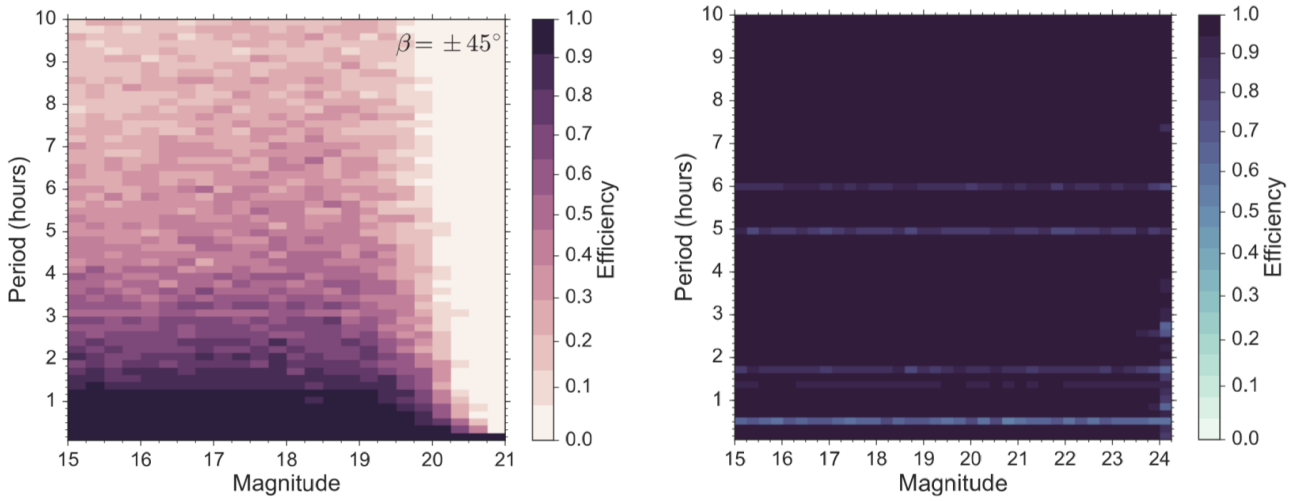

Figure 15: Detection efficiency of Gaia versus LSST. (a) Gaia mainly detects bright binaries. The shorter the period the easier to detect as they spend longer time in the eclipse phase. (b) LSST even detects fainter binaries and has a higher efficiency, which is because LSST detects each object much more frequently than Gaia does (Korol et al. (2017)).

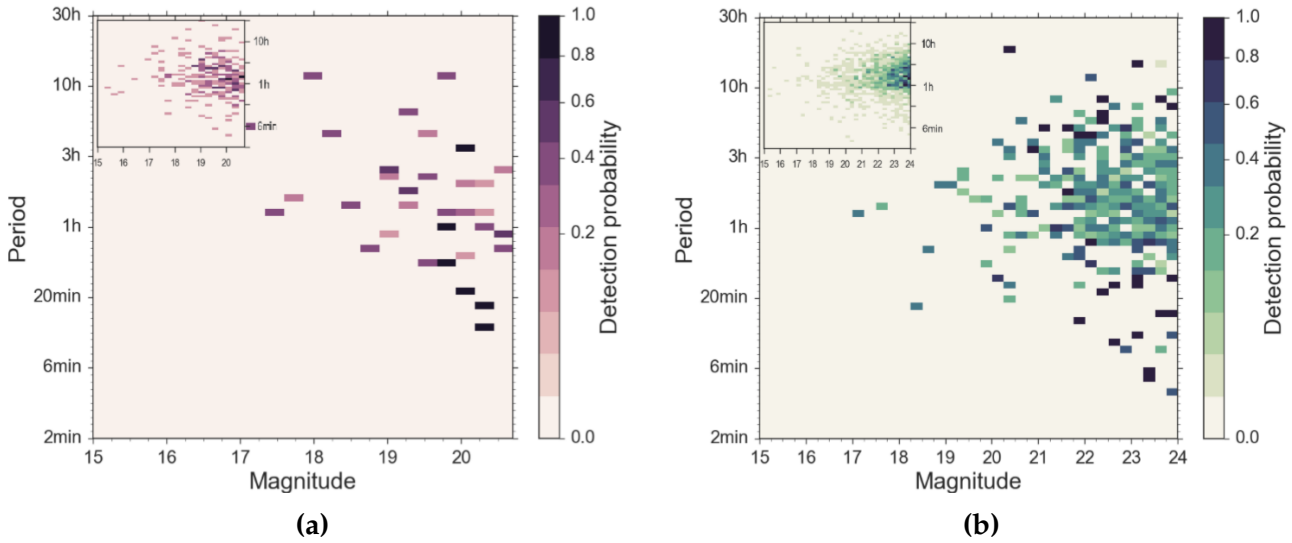

Figure 16: Detection probability from the population was simulated for Gaia versus LSST. (a) Gaia detecting binary magnitudes < 21. (b) LSST also detecting fainter binaries with magnitudes < 24 (Korol et al. (2017)).

Detection efficiency was simulated using average values for the population parameters ($m_1 = 0.53M_\odot, m_2 = 0.35M_\odot, R_2 = 0.017R_\odot, R_1 = 0.8R_2, d = 1kpc$ and $i = \pi/2$). The number of times the light curve was detected with photometric variability that occurs at eclipses was simulated for Gaia and for LSST. Respective results for a limited time are shown as detection efficiency in Fig. 15. Gaia (a) mainly detects bright binaries. Binaries with short periods are more detectable because they spend a longer time in the eclipse phase. The result for LSST (b) shows that it has high detection efficiency regardless of period and magnitude.

LSST also detects lighter objects, but its superior efficiency is because LSST detects each object much more frequently than Gaia does. The bright lines show that the efficiency is lower when the orbital period is in phase with the cadence of observation.

Furthermore, a detection probability survey was conducted, where the simulated population was representing the Galaxy was used for Gaia and for LSST (Fig. 16). It is also presented as period versus magnitude diagrams. For the simulation of Gaia, 190 binaries were found to have a non-zero detection probability and the most remote detected binaries have a distance of 3.5 kpc. For LSST, 1100 binaries were found to have a non-zero probability and the most distant have a distance of 10 kpc. When comparing to Fig. 15, it shows that Gaia is more efficient at detecting brighter systems but the majority of the detected population is faint. LSST can detect a much larger portion of the population. However, those that are faint have much poorer astrometric accuracy and are much more difficult to perform spectroscopy on.

3.2.4 Binaries detected by LISA

Also, the same simulation was made for LISA, using the same population as for previous tests together with known verification binaries. The number of observed binaries with SNR > 7 is for one year of mission $\sim$ 10 000 and for four years of mission $\sim$ 25 000. Fig. 17 shows diagrams where period, mass, distance, and Galactocentric distance are related to magnitude. Comparing the period/magnitude diagram for LISA with the corresponding diagram for Gaia and LSST in Fig. 16, it shows that LISA can detect significantly fainter binaries with magnitude up to the test value 70. Though, LISA will mainly detect objects with short periods. The chirp mass according to the test can be measured up to $1 M_{\odot}$ but most of the masses detected are significantly smaller.

LISA mostly detects binaries at a distance of 10 kpc, which is the maximum limit for the measurement values for binaries for LSST. Using a simulation that is adapted to the Galaxy, many detected binaries are close to us. There is a wide range of magnitude for the detected binaries at the center of the Galaxy at 8 kpc, as the bulge contains many objects. LISA can detect objects in the bulge as well as beyond the bulge near the extension of the Galactic disc. However, the stellar disc extends to the distance of 30 kpc and looking at the figure, no binary seem to be detected this far out, which does not match other expectations of LISA's capability. They also investigated what Gaia and LSST can detect in the Galaxy. In particular, Gaia can see binaries with distances < 3.5 kpc. LSST, which can see further, will give a better picture of the distribution of binaries in the Galaxy but not in and beyond the bulge the way LISA can. Though, LSST can detect individual brighter stars all over the Galaxy but with some limitations in crowded too bright areas such as the bulge.

The paper describes that from only using electromagnetic data, measurable parameters are orbital period, inclination angle and scaled radii of the binary. From those values, the binary mass ratio can be determined. For synergy effects with LISA measuring the chirp mass, the respective mass of the stars can be calculated. LISA will also provide information on which objects are binary and which are not binary, which is essential for using the electromagnetic data correctly.

Data from LISA will open up great opportunities to study the final stage of binary evolution. A white dwarf binary can fuse and can then give rise to a rare star, a neutron star or it can explode like a type Ia supernova. The binaries that have orbital periods of just minutes

or hours give opportunity to study tidal forces, to calculate which substances the systems consist of and their development of time of detection.

The project has shown that the hopes of LISA's success are high. Many binaries will be detected by both electromagnetic and gravitational waves, providing important multi-messenger astronomy for future scientific research (Korol et al. (2017)).

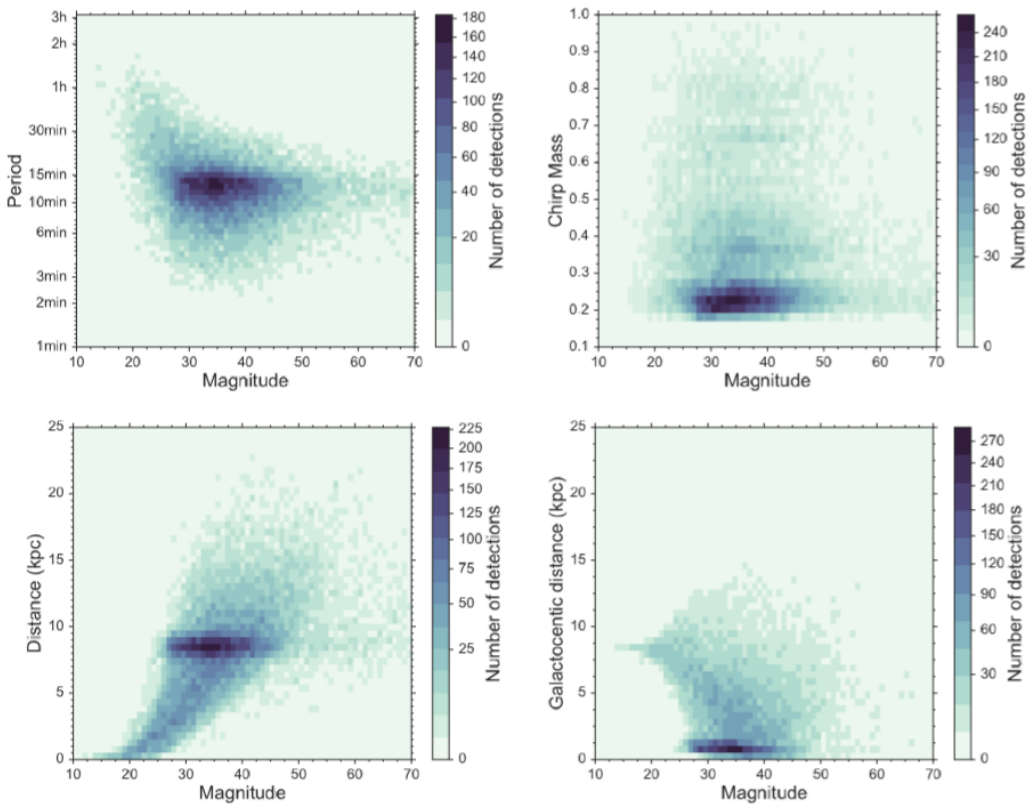

Figure 17: LISA detections for SNR > 7. Diagram where period, mass, distance, and Galactocentric distance are related to magnitude. LISA can detect faint binaries for short periods and can detect objects on the other side of the center of the Galaxy (Korol et al. (2017)).

3.3 Encapsulation of the paper; A multimessenger study of the Milky Way's stellar disc and bulge with LISA, Gaia, and LSST

Valeriya Korol, Elena M. Rossi, and Enrico Barausse, 2019 (Korol et al. (2019)).

3.3.1 Introduction

The white dwarf binaries will make up the majority of binaries that LISA will detect in the Milky Way. According to this paper written later than the previous paper, LISA is expected to observe even more of them, approximately 10^5, of which almost 80 are verification binaries, providing synergy effects.

The paper is a sequel to the previous paper, also made by the V. Korol team. It examines the precision of LISA distance measurement and its ability to recreate the density profile of the stars in the Milky Way. Simulations are made by a synthetic population of the Milky Way,

including the bulge, the stellar disc and the dark matter halo to correspond to the Galactic kinematics.

3.3.2 LISA detection and distance with errors

LISA has the ability to detect binaries in the bulge, which is not possible with electromagnetic measurements. However, overlapping signals are recorded by LISA from high-density areas. It provides a stochastic background signal instead of information on specific resolvable binaries. Still, it will provide useful information such as to calculate the Galactic stellar population, baryonic content, and shapes. In the project, however, only resolvable detectable binaries are handled, with a focus on detached binaries (see Fig. 11).

In the previous project, two different scenarios of phases of mass transfer between the stars in the binaries were used, but this time only the one that includes loss of energy, in the form of mass and angular momentum, is used. This is because this project focuses on the spatial distribution of binaries, which is not affected by it. The Galaxy's velocity distribution of energy and angular momentum is recreated, where the bulge dominates the dynamics closest to the center, the disc dominates the dynamics further out, and the halo even further out, far beyond the position of the Sun. For binaries, the gravitational wave is described, based on the orbital period (P) and the chirp mass (M_c), as the quadrupole approximation (τ) as

$$\tau \approx 1Myr(\frac{P}{12min})^{(8/3)}(\frac{M_c}{0.3M_\odot})^{(-5/3)}, \tag{8}$$

which was used for the simulation. Further, the amplitude can be described as in equation 6 but also as a function comprising the frequency derivative (f') as

$$A = \frac{5}{96\pi^2}\frac{f'}{f^3 d}\ , \quad f = 2/P. \tag{9}$$

The frequency derivative is described as

$$f' = \frac{96}{5}\pi^{(8/3)}(\frac{GM_c}{c^3})^{(5/3)}f^{(11/3)}. \tag{10}$$

Combining equations 8 to 10, distance with measured values from LISA can be calculated. This is true for detached binaries. For accreating AMCVns, which are not included in the simulation, the formula also includes components that describe mass transfer or tides, that cannot be measured by LISA without additional electromagnetic observations from Gaia or LSST. How this could be solved is not described in the paper. For mapping of the Milky Way at a distance that extends beyond Gaia and LSST's range for binaries, only detached binaries can be used. The frequency of AMCV binaries decreases with the evolution of time due to the mass transfer, while the frequency of detached binaries increases due to gravitational wave emission (meaning that the orbital period decreases). Since LISA is also in motion, all measurement values must be adjusted to a reference frame that relates to the Sun.

According to the simulation, it is estimated that LISA will detect approximately 10^5 binaries with SNR > 7, of which the majority, $2.6 \cdot 10^4$, are double white dwarfs. The white dwarf binaries are illustrated in Fig. 18. The signals are strongest for close-up objects, but

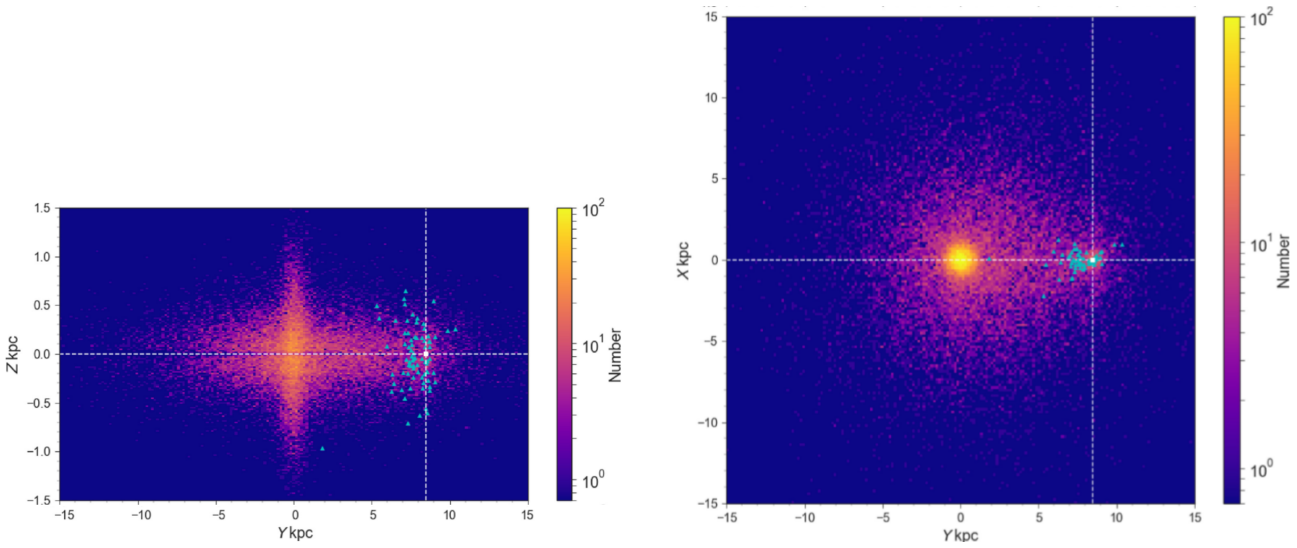

(a) **(b)**

Figure 18: Results of detected LISA binaries according to simulation. The white square illustrates the Sun. The turquoise dots are verification binaries detected by Gaia and LSST. Most binaries, detected by LISA are in the bulge. (a) X-Y plane (b) Z-Y plane (Korol et al. (2019)).

binaries at distances greater than 15 kpc from the center of the Galaxy can also be detected. For uncertainties for distance calculation, the respective errors from the variables A, f and f' are added together. 30% of the detected binaries meet the quality requirement σ_d/d, which should be < 30 %.

The same simulation for Gaia and LSST yielded respectively 25 and 75 detected verification binaries. Only a few of the binaries detected by Gaia, were not detected by LSST. All binaries are detected only at a short distance compared to LISA. The uncertainty for parallax for Gaia has expected error < 20 % and just as for LISA, represents 30 % of their catalog.

The errors were computed with the results, as Fig. 19a illustrates, where observed distances are a function of the true distances for all three telescopes. The blue markers represent electromagnetic calculations with parallax, while the purple markers are from gravitational waves. The values from Gaia and LSST follow the line where $d_{obs} = d$ up to 2 kpc but then the calculations are incorrect for longer distances, where instead LISA gives better results. However, by combining the measurement values from each telescope, it is possible to choose the best values and reduce uncertainty. The mean of the three telescopes can be calculated for distance as

$$d_{GW+EM} = \frac{d_{GW}\sigma_{EM}^2 + d_{EM}\sigma_{GW}^2}{\sigma_{EM}^2 + \sigma_{GW}^2}, \tag{11}$$

with error as

$$\sigma_{GW+EM} = \left(\frac{\sigma_{EM}^2\sigma_{GW}^2}{\sigma_{EM}^2 + \sigma_{GW}^2}\right)^{(1/2)}. \tag{12}$$

In the graph Fig. 19b it appears to be not only a result of the equation but also removed values.

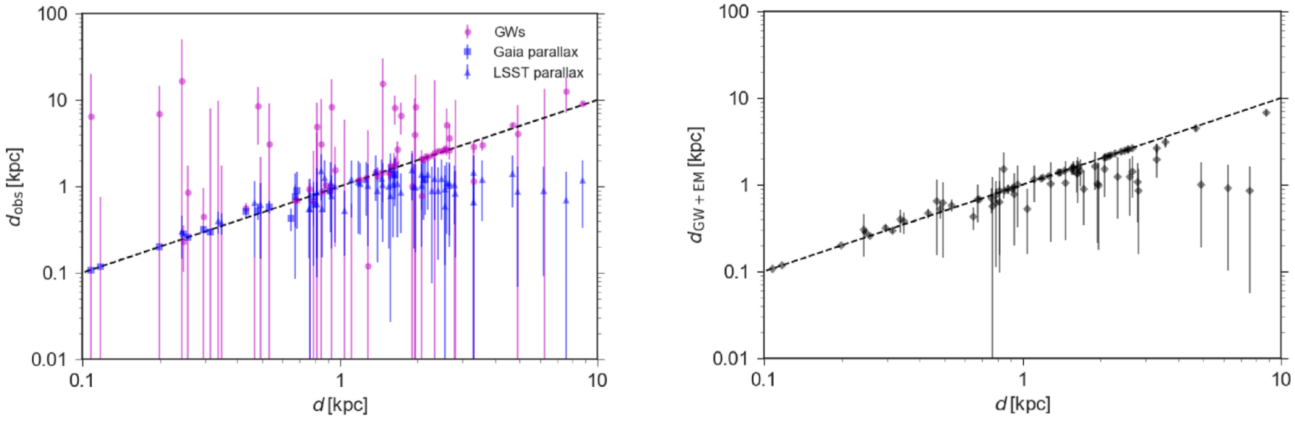

(a) **(b)**

Figure 19: Observed distance values from Gaia, LSST and LISA, as a function of the true distance. For dotted line $d_{obs} = d$. (a) Distance estimates from electromagnetic observations are blue (Gaia with squares and LSST with triangles) counted from parallax, and gravitational waves are purple. (b) The measured values are combined in this graph, which gives improved results and error margin (Korol et al. (2019)).

3.3.3 Density distribution map with LISA

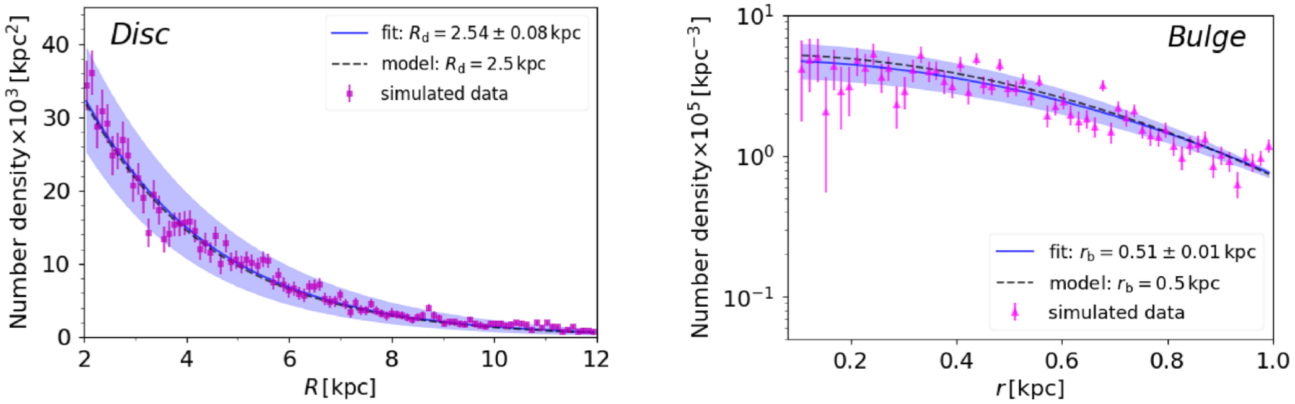

(a) **(b)**

Figure 20: Number density as a function of radius. The purple points are simulated data. They follow a best-fitting curve in blue. Their error follows the light blue surface. (a) Number density $\times 10^3/kpc^2$ as a function of the cylindrical radius R plotted for the disc. (b) Number density $\times 10^5/kpc^3$ as a function of the spherical radius r plotted for the bulge (Korol et al. (2019)).

LISA measurement values will be used to make a density distribution map of white dwarfs in the Galaxy. To test this possibility, the simulation that is illustrated in Fig. 18

is used, included relative error < 30 % (which gives 30 % of the detected binaries). Number density, as a function of the radius, is plotted in Fig. 20 for the disc (a) and for the bulge (b) separately. For the disc seen from above, the purple simulated values follow a best-fitting line in blue, which is constituted by a curve comprising the function constant scale radius R_d. The resulting value of R_d is 2.54 ± 0.08 kpc, which is ~ 3 % precision of the correct value of 2.5 kpc. The bulge is assumed to have a spherical population in the inner ~ 2 kpc. The same method for the bulge gave an even better result of the scale radius. This means that LISA is well placed to distinguish density profiles.

3.3.4 Kinematics and rotation curve for Gaia and LSST

White dwarfs are too lightweight to measure velocity with radial velocity spectrometers for Gaia and LSST. Though, the their rotation speed around the Galaxy can be calculated from only the proper motion (μ_{obs}) from electromagnetic data, which depends on relative velocity in proportion to the distance. A simulation was done for the mock Galaxy, from which the observed velocity is described as

$$V_{obs}(R) = \frac{R}{d_{obs} - R_0 cosl}(4.74\mu_{obs}d_{obs} + V_0 cosl) \quad km\ s^{-1}, \tag{13}$$

where R is the position vector for the observed binary (Fig. 21a), l is the angle and V_0 is the velocity vector corresponding to the circular velocity around the center of the Galaxy, $V_{circ}(R)$. The observed velocity $V_{obs}(R)$ is simulated for each binary with the respective error with results according to Fig. 21b where $V_{circ}(R)$ is a function of the radius.

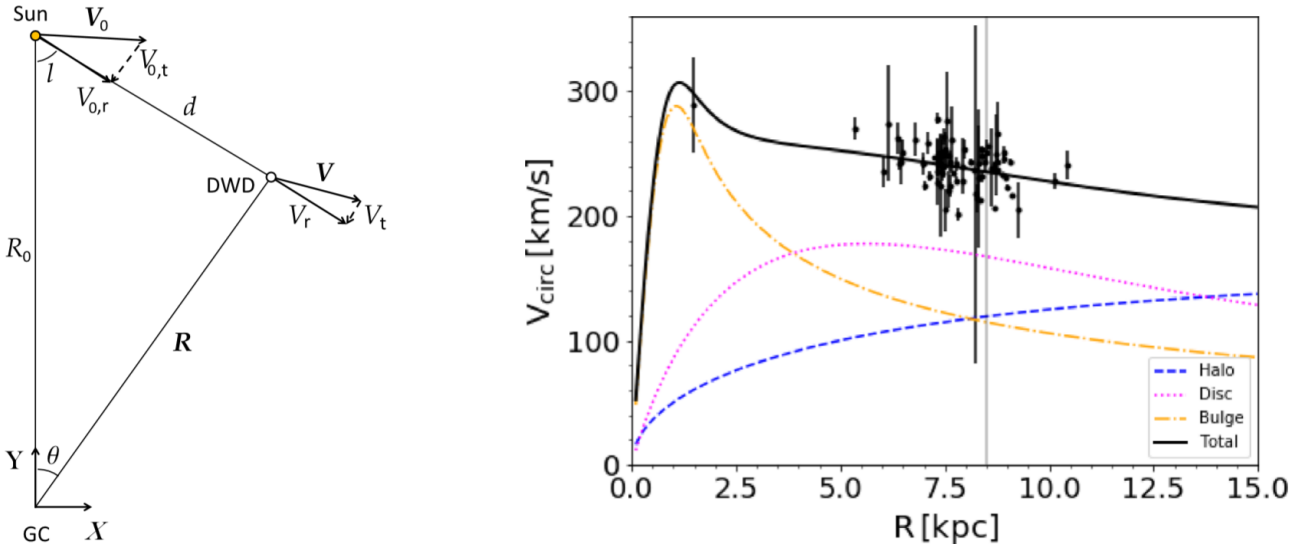

(a) **(b)**

Figure 21: (a) Kinematic model for any binary simulated. GC stands for the Galactic center. (b) The rotation speed of binary as a function of radius. The black line is the simulated rotation curve that represents the total speed of objects in the bulge (yellow), the disc (red) and the halo (blue). The points are the detected binaries. The vertical line marks the position of the Sun (Korol et al. (2019)).

The black line is the rotation curve which constitutes the observable speed in the direction V_0 for objects in the bulge (yellow), the disc (red) and the halo (blue). The simulated lines look like the rotation curves are described for all objects in the Galaxy. Near the center is $V_{circ}(R) = 0$, since all objects move in any direction. After the maximum point, the curve would fall rapidly if dark matter was not present. The points are the detected binaries, which are local since they are detected by Gaia and LSST.

The investigation also provided that based on multi-messenger data it is possible to calculate the dark matter halo of the Galaxy and to search for its historical content of dark matter. Dark matter information is fundamental to understanding the Galactic rotation curve. The test result was uncertain but it can be improved with access to Gaia's final complete data. Many parameters are needed to make proper kinematic calculations for binaries, and LISA is needed. Further calculations showed that accelerations and Doppler terms are not large enough to affect LISA's measurements.

3.3.5 Prospects based on the project

The bulge mass can be calculated from the Galactic rotation curve, together with the distances between binaries detected by LISA, and proper motions from the optical telescopes. In the center of the Milky Way, the bulge comprises most of the mass of the Galaxy. LISA will thus be an important part of the mapping of the structure of our Galaxy.

Both sides of the Galaxy will be mapped with a small margin of error and the baryonic mass of both the stellar disc and the bulge will be calculated. It should be taken into account that the study was done on a simplified simulation of the Milky Way without spiral arms and density asymmetry. Also, the population could be more realistic by adding AMCVn white dwarfs to the calculations even though they form a minor part of the binaries. A more detailed simulation of the Galaxy would improve the result. Although, this project is already providing useful information about the possibilities (Korol et al. (2019)).

3.4 More papers, written by the V. Korol team about LISA

3.4.1 White dwarfs and exoplanets with LISA

Another new paper, written by V. Korol team, considers LISA's ability to detect brown dwarfs and exoplanets that are orbiting double white dwarf binaries. A simulation with different combinations of mass and axis has shown that LISA has good conditions for detecting these throughout the Milky Way and possibly also in nearby galaxies in the Local Group. In the region that is detectable for Gaia and LSST, it provides a strong opportunity for multi-messenger research (Danielski et al. (2019)).

3.4.2 Detection within the Local Group with LISA

Satellite galaxies of the Milky Way were explored in one paper. According to the results of the simulation, the number of detected binaries depends strongly on their mass. The frequency needs to be > 3 mHz to be detected. This time, different metallicity of the stars was used for the simulations. It did not show to affect the evolution of population of white

dwarfs very much. The number of binaries was increasing slightly for a decreasing metallicity. (Korol et al. (2020)).

Opportunity to explore the Local Group is examined in another paper. Computer simulation gives the relation between distance, orbital period and chirp mass with the result that LISA can mainly make many observations in the Large and Small Magellanic clouds (P < 20 min) but is expected to be able to make observations throughout the Local Group. LISA can find between ten to several tens of binaries in the Andromeda galaxy. These will be those with the shortest orbital periods and largest mass ($P < 10$ min and $M > 0.5\ M_{\odot}$), which are conducive to merge as a Type Ia supernova (Korol et al. (2018)).

4 Papers from other authors about Gaia, LSST and LISA

Multi-messenger effects about Gaia, LSST and LISA, which are presented in papers that are not written by V.Korol, are described below.

4.1 Multi-messenger observations for calculation of mass

4.1.1 Calculation of mass from multi-messenger

A project, presented in the paper (Breivik et al. (2018)), describes multi-messenger effects for the accreting mass-transferring binaries, which make up most of the verification binaries. For all circular binaries, signal-to-noise ratio (S/N) can be described as

$$S/N \approx \frac{h_0\sqrt{T_{obs}}}{h_f}, \tag{14}$$

where T_{obs} is the observational time of LISA mission and h_f is the spectral amplitude value for a specified frequency of a gravitational wave, f_{GW}, that is given by the standard LISA sensitivity curve. h_0 is a scaling amplitude,

$$h_0 = 4\frac{G}{c^2}\frac{M_c}{d}(\frac{G}{c^3}\pi f_{GW} M_c)^{(2/3)}, \tag{15}$$

where M_c is the chirp mass according to equation 7 and d is the distance. For detached binaries, chirp mass is calculated using only LISA's measured values, but for mass transfer AMCVn binaries, these equations are useful for calculating chirp mass and then the distance from multi-messenger data is needed. This can be achieved if Gaia or LSST has been able to measure parallax.

AMCVn binaries consist of a helium-rich donor star and an accretor star. These systems can be AMCVn or future Type 1a supernova. Verification binaries with He-donors detected by Gaia are illustrated in Fig. 22a showing detection number as a function of the orbital period for He-donor binaries. The simulation yielded 3000 detected binaries for LISA and 80 for Gaia. Of these, 60 were verification binaries, of which distance, d, can be calculated.

4.1.2 The relation to the frequency

The project shows that there is an important relationship between donor mass, M_D, and the frequency of gravitational waves f_{GW}. f_{GW} is determined by the orbital frequency f_{orb}.

Fig. 22b shows the donor mass versus frequency with a negative derivative, called chirp (f'). Chirp mass M_c is a definite result of energy loss from the transmission of gravitational waves. Using these relationships and the chirp then mass transfer rate and donor mass can be determined. Knowing donor mass and chirp mass, from multi-messenger observations, then the accretor mass can be calculated with equation 7. This means that is easier to measure chirp mass than the two masses separately. The relationships rely on the fact that the radius is a function of the mass and chemical composition.

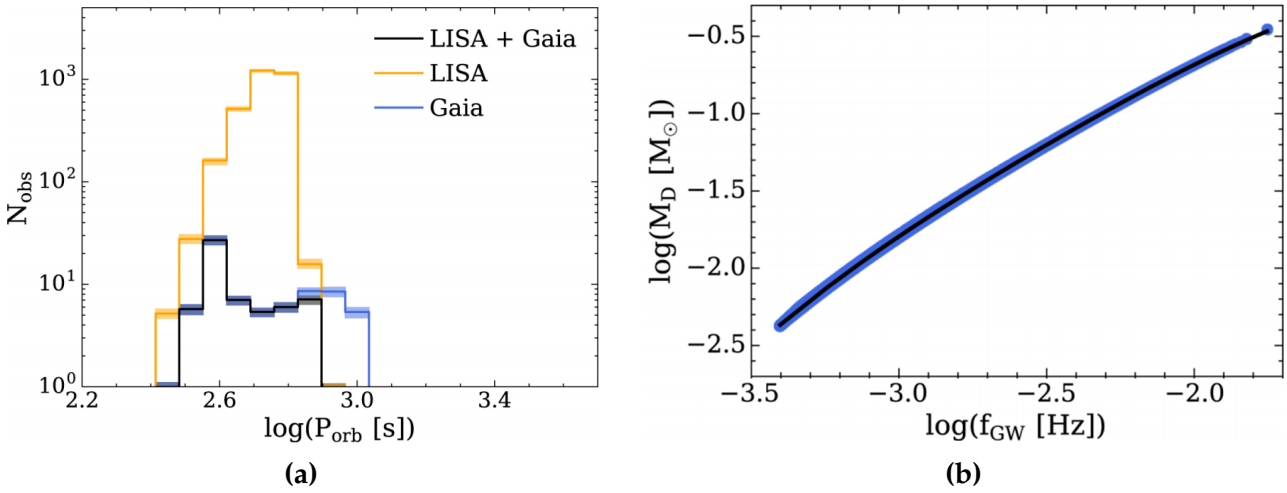

Figure 22: (a) Number of observations of mass-transferring binaries, considering orbital period in seconds. Verification binaries detected by LISA and Gaia (black line). Chirp mass can only be calculated if the object also can be detected by electromagnetic telescopes, giving the parallax. (b) Donor mass versus frequency with a negative derivative, called chirp (f') (Breivik et al. (2018)).

Chirp (f') can be divided into three parts as

$$f'_{total} = f'_{GR} + f'_{MT} + f'_{tides}, \tag{16}$$

where f'_{GR} is the frequency of gravitational radiation, f'_{MT} is the frequency of mass transfer and f'_{tides} is the frequency of tidal interaction (Breivik et al. (2018)).

4.2 Metallicity and age with LISA

Another author, A. Lamberts, writes that other studies are predicting that Gaia will detect about 25 verification binaries and LSST will add 50 more. These studies are, according to the author, missing the metallicity and age properties of the stars in their simulations, and that is what was added and studied in this project. Results show that LISA will detect 50 % He-CO binaries, 30 % He-He binaries, 20 % CO-CO binaries and a few percent binaries with a Ne white dwarf. The He-He binaries are mostly detected in older stellar populations, such as the bulge, the thick disc and in the stellar halo. CO-CO and Ne-X binaries are more commonly detected in younger stellar populations in the thin disc (Lamberts et al. (2019)).

4.3 Multi-messenger possibilities with black holes

One model shows that LISA will detect at least 20 binary black holes. The chirp mass separates them from white dwarfs. Multi-messenger astrophysics may be possible even with black holes. LISA finds the binaries and then electromagnetic signatures may be found at the site, telling about their history. Or, on the contrary, microlensing surveys allow LISA to find them (Tauris (2018)), (Lamberts et al. (2018)), (Sesana et al. (2020)).

4.4 Multi-messenger with neutron stars using LISA and SKA

LISA is also expected to observe tens of neutron star binaries. They can also be detectable as radio pulsars. There are possibilities for multi-messenger observations with the planned radio telescope Square Kilometers Array (SKA). This may happen to ultra-relativistic binaries with a period < 400 s. They are expected to be detected first by LISA and then separated from other signals by SKA and its evolution can be studied (Thrane et al. (2020)).

5 Papers about Gaia and LSST

5.1 Uncertainty values for Gaia and LSST

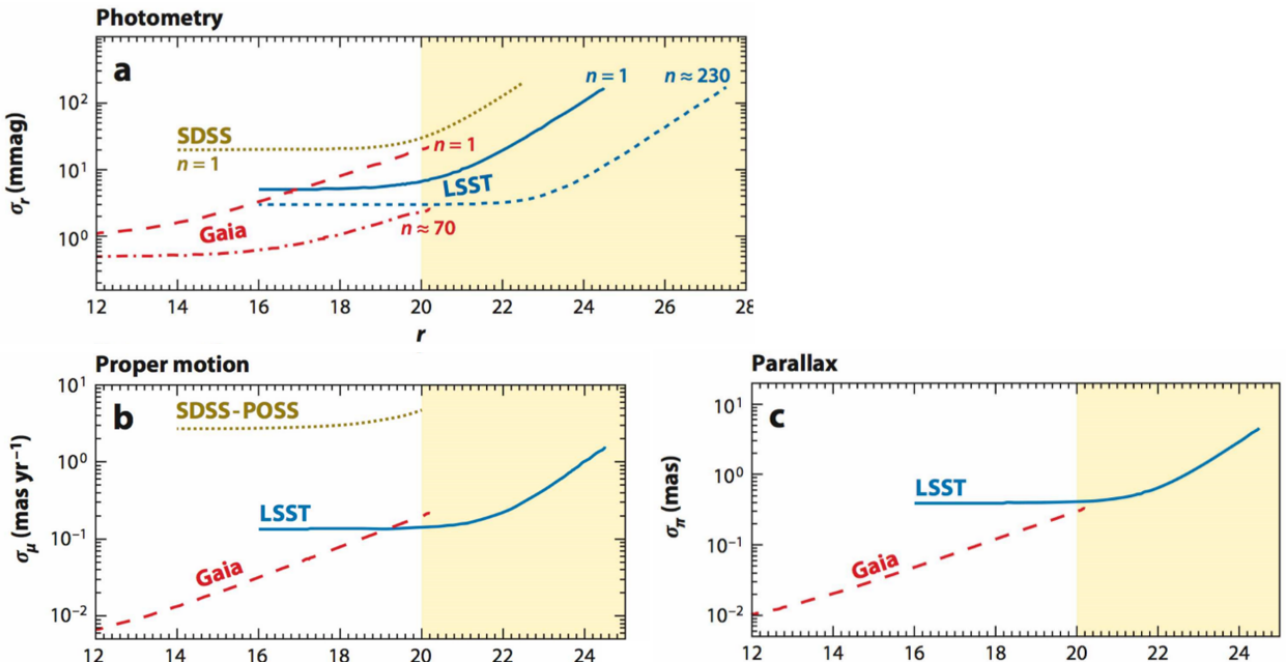

Figure 23: The uncertainty for photometry, proper motion and parallax as a function of magnitude for Gaia and LSST. For photometry, the result is shown for both one and for many observations. The error margins are larger for the SDSS telescope (Ivezić et al. (2015)).

LSST can be regarded as a complement to Gaia. Both Gaia and LSST use photometry and astrometry. Fig. 23 illustrates the error margins for photometry as well as proper motion and

parallax, which is measured by astrometry. It gives a clear picture of how the measurement values for LSST become better at the magnitude 19-20 where Gaia's measurement values become worse, just below the limit of the magnitude that Gaia can measure. The images also show Gaia's superb quality for bright stars, which LSST cannot offer. LSST's unprecedented ability is instead to measure faint objects. The uncertainties are quite similar for both of them and the overlap between them gives one fairly smooth curve. For the objects that can be measured by both, the margin of error can be further minimized with the multi-messenger effect, which is previously described in chapter 3.3.2 (Jurić & Ivezić (2010)), (Eyer et al. (2012)), (Ivezić et al. (2015))

5.2 Photometric calibration synergy

Gaia's data can be used to improve the calibration of the LSST photometric values. Using known objects, then Gaia's G band calibrate LSST's 6 separate bands u, g, r, i, z and y, each coming from the different filters, shifted by the camera. Since they have 1 and 6 bands respectively, their values look different, as shown in Fig. 24. However, they can be transformed into each other so that they become comparable. It improves object verification, cross-calibration and error margins (Axelrod & Miller (2014)), (Clementini et al. (2018)).

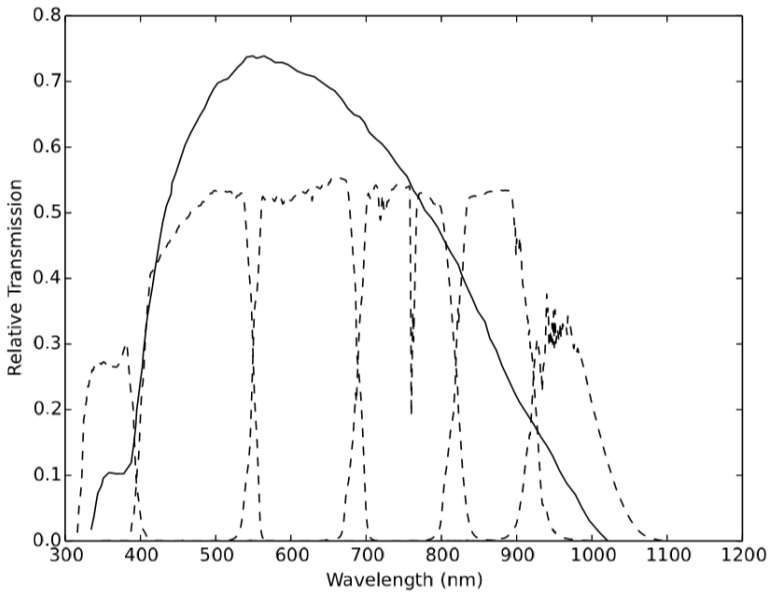

Figure 24: Bandpasses for Gaia's G band (solid line) and for LSST's u, g, r, i, z, and y bands (dotted line). Relative transmission versus wavelength (Axelrod & Miller (2014)).

6 Discussion

There are many papers about the telescopes but only a limited amount is about the synergy-effect. Above all, it is V. Korol's team whose project is about comparing the telescopes and highlighting the synergy opportunities. Thus other authors refer to V. Korol. Both theory and methods are simplified and not always clearly explained, which means that it is difficult to give detailed criticism. In general, it can be stated that the simulations in the papers are

a simplified picture of the Galaxy, with limited details for certain stellar populations. In addition, they are based on assumptions. All the simulations thus give different results and should be regarded as a valuable guidance for what can be expected. If a project has found 50 or 80 verification binaries for a certain signal-to-noise value, then there is no major difference. The important thing is that it looks promising to find verification binaries that will be used to perform multi-messenger astronomy.

7 Conclusion

LISA will make it possible to detect binaries in the bulge and beyond, even outside of the Galaxy. It will become possible to study the final state of evolution of binaries, density distribution, tidal forces and so much more. Expectations are great for what the telescope can teach us about the Universe.

Many computer simulations have been done to identify the detection possibilities of white dwarf binaries. From these, Gaia is expected to detect 190 binaries, LSST 1100 binaries and LISA 10^5 binaries. Verification binaries, which can be observed with both electromagnetic and gravitational waves, can be used to make multi-messenger observations. About 25 of these have been noted by Gaia and another 50 by LSST. More are expected to be found, but the defined verification binaries are likely to be detected at an early stage as they have a high signal-to-noise value. There are many examples of the possibility of a synergy effect:

- LISA will be able to detect which are binaries of the objects found by optical telescopes, so the optical data can be used correctly. Collaboration between Gaia and LSST can also improve object verification. Cross-calibration will also be a useful method.

- Gaia uncertainty is high for faint objects while LSST uncertainty is high for bright objects in their overlapping magnitude range. This is because LSST is designed to detect faint objects with longer wavelengths, detecting each object more frequently and using 6 different filters. Together, Gaia and LSST provide a smooth uncertainty curve in relation to distance. Comparing measurement values from different measurement methods always means smaller error margins, in a similar way that more measurement values do. However, multi-messenger calculations with optical and gravitational measurements can improve the values for distance and uncertainty.

- The chirp mass for AMCVn binaries can be calculated using optical values of parallax together with LISA's values for amplitude, frequency and more. Similarly, the stars and mass transfer rate can be calculated for verification binaries. Without Gaia and LISA, distances can only be calculated for detached binaries by LISA. This means that only the AMCVn binaries, detectable by both methods, will contribute to the mapping of the Milky Way.

- Thus, the method used to calculate the distance with LISA values can also be used for AMCVn binaries with more data from synergies with optical telescopes to handle the mass transfer. This means that distance can then be calculated both by this method and by parallax.

- The bulge mass can be calculated using the distance between binaries from LISA and proper motions from optical telescopes.
- Black hole and neutron star binaries can also be studied with multi-messenger astronomy. Also brown dwarfs and exoplanets, orbiting white dwarf binaries, can be examined.
- Multi-messenger data can also be used to investigate evaluation of galaxies and dark matter halo. It can give a better understanding of what dark matter is, that may explain the ever-mysterious Galactic rotation curve. Synergy-effect will help understanding the Universe.
- There are also multi-messenger possibilities with LISA in combination with other kinds of a telescope, such as radio telescope SKA (Square Kilometers Array). The synergy possibilities will increase.

8 Acknowledgement

I am grateful to the wonderful supervisor David Hobbs.

References

Axelrod, T. & Miller, C. 2014, PASP, 126, 1102

Bailer-Jones, C. A. L. 2015, PASP, 127, 994

Breivik, K., Kremer, K., Bueno, M., et al. 2018, ApJ, 854, L1

Clementini, G., Musella, I., Chieffi, A., et al. 2018, arXiv e-prints, arXiv:1812.03298

Danielski, C., Korol, V., Tamanini, N., & Rossi, E. M. 2019, A&A, 632, A113

Egberts, K. 2020, arXiv e-prints, arXiv:2004.12460

Eyer, L., Dubath, P., Mowlavi, N., et al. 2012, in IAU Symposium, Vol. 282, From Interacting Binaries to Exoplanets: Essential Modeling Tools, ed. M. T. Richards & I. Hubeny, 33–40

Gaia Collaboration, Babusiaux, C., van Leeuwen, F., et al. 2018a, A&A, 616, A10

Gaia Collaboration, Brown, A. G. A., Vallenari, A., et al. 2018b, A&A, 616, A1

Gaia Collaboration, Prusti, T., de Bruijne, J. H. J., et al. 2016, A&A, 595, A1

Gaia Helpdesk, E. 2020, Gaia DR2 primer, issue 1.1, 17

Ivezić, Ž., Kahn, S. M., & Eliason, P. 2015, arXiv e-prints, arXiv:1502.06555

Jurić, M. & Ivezić, Ž. 2010, in EAS Publications Series, Vol. 45, EAS Publications Series, 281–286

Korol, V., Koop, O., & Rossi, E. M. 2018, ApJ, 866, L20

Korol, V. & Rossi, E. M. 2019, in The Gaia Universe, 56

Korol, V., Rossi, E. M., & Barausse, E. 2019, MNRAS, 483, 5518

Korol, V., Rossi, E. M., Groot, P. J., et al. 2017, MNRAS, 470, 1894

Korol, V., Toonen, S., Klein, A., et al. 2020, arXiv e-prints, arXiv:2002.10462

Kupfer, T., Korol, V., Shah, S., et al. 2018, MNRAS, 480, 302

Lamberts, A., Blunt, S., Littenberg, T. B., et al. 2019, MNRAS, 490, 5888

Lamberts, A., Garrison-Kimmel, S., Hopkins, P. F., et al. 2018, MNRAS, 480, 2704

Lindegren, L. & Hobbs, D. 2018, Dynamical astronomy Lecture notes for ASTM13, updated by David Hobbs for Gaia DR2 (Lund University)

Schneider, P. 2015, Extragalactic Astronomy and Cosmology an Introduction, second edition (Springer)

Sesana, A., Lamberts, A., & Petiteau, A. 2020, MNRAS, 494, L75

Tauris, T. M. 2018, Phys. Rev. Lett., 121, 131105

Thrane, E., Osłowski, S., & Lasky, P. D. 2020, MNRAS, 493, 5408

van Leeuwen, F., de Bruijne, J. H. J., Arenou, F., et al. 2017, Gaia DR1 documentation, Gaia DR1 documentation